# Photoelectron Dynamics in X-Ray Free-Electron-Laser Diffractive Imaging of Biological Samples

Stefan P. Hau-Riege

Phys. Rev. Lett. **108**, 238101 — Published 4 June 2012

DOI: 10.1103/PhysRevLett.108.238101

# The role of photoelectron dynamics in x-ray-free-electron-laser diffractive imaging of biological samples

Stefan P. Hau-Riege*
*Lawrence Livermore National Laboratory, Livermore, CA 94550*
(Dated: May 4, 2012)

X-ray free electron lasers hold the promise of enabling atomic-resolution diffractive imaging of single biological molecules. We have developed a hybrid continuum–particle model to describe the x-ray-induced damage and found that the photoelectron dynamics and electrostatic confinement strongly affect the time scale of the damage processes. These phenomena are not fully captured in hydrodynamic modeling approaches.

PACS numbers: 87.64.Bx,87.59.-e

## INTRODUCTION

X-ray free electron laser (XFELs) may enable atomic-resolution diffractive imaging of single, isolated biological molecules [1]. Recently, rapid progress has been made toward this goal: Seibert *et al.* imaged single mimivirus particles [2], Chapman *et al.* demonstrated high-resolution femtosecond protein nanocrystallography [3], and Frank *et al.* pioneered diffractive imaging from two-dimensional protein crystals [4]. First experiments on radiation damage showed Bragg spot fading in lysozyme and Photosystem I nanocrystals at an x-ray energy of 2 keV [5, 6] that worsens with increasing pulse length. Radiation damage was observed for pulses as short as about 40 fs [5]. Since without Bragg enhancement non-periodic samples require significantly larger x-ray fluences than nanocrystals to achieve acceptable signal-to-noise ratios [7], x-ray radiation damage is expected to continue to severely limit the achievable image resolution.

X-ray damage is initiated by inner-shell photoionization, leading to the emission of high-energy photoelectrons that carry most of the absorbed x-ray energy. For example, in carbonous molecules about 90 % of all interactions with 8 keV x rays are photoionization events, and the emitted photoelectrons have a kinetic energy of about 7.3 keV. Since fast photoelectrons can leave the sample, their dynamics determine the charge re-distribution. Photoelectrons that stay in the vicinity of the sample transfer their kinetic energy through inelastic scattering (stopping) that increases the sample's temperature and ionization state. The associated damage mechanisms that degrade the diffraction pattern are atomic form factor modifications through ionization, local atomic re-arrangements due to bond breaking and microfields in the nanoplasma, hydrodynamic expansion due to electronic heating in the sample, and Coulomb explosion caused by charging associated with the escape of fast electrons. The first three of these processes depend on the amount of energy transferred from the photoelectrons to the sample, whereas the latter depends on the photoelectron trajectories. Other atomic processes that generate slow electrons which are electrostatically confined to the sample (*trapped*) are Auger decay, collisional ionization, three-body recombination, and field ionization.

Both particle [1, 8–11] and transport models [12–15] have been proposed to describe the evolution of x-ray irradiated materials. The former treat electrons and ions as particles and calculate their trajectories by solving Newton's force equations every time step. All-particle molecular dynamics models are computationally expensive and therefore limited to small biological samples. Transport models describe the evolution of larger systems by using collective density functions. An example are hydrodynamic models, for which it is assumed that an electron temperature is well defined, so that the electron distribution function can be assumed to depend only on position and time [12]. This type of model has been popular for analyzing recent experiments on nanocrystals [6, 15], but they do not treat the non-thermal photoelectron dynamics correctly since they assume complete trapping of electrons and instant thermalization. The assumption of complete trapping is often reasonable for very large samples, such as macroscopic solids [10], because the range of the photoelectron is smaller than the sample dimension, or because the photoelectrons are electrostatically trapped due to large positive charge buildup. In this paper we show that both assumptions are not necessarily correct for biological imaging experiments, especially for harder x rays, since trapped electrons are generally confined only to the vicinity of the sample and not to the sample itself, and therefore the thermalization time is often much longer than the x-ray pulse duration. More advanced Boltzmann-type model consider the velocity-dependence of the electron distribution function [14] and could, in principle, correctly treat the photoelectron dynamics, but that would require including higher Legendre modes to be included in their description than it is currently done [14].

To summarize, most relevant samples are too large for an all-particle treatment, and the fast photoelectron dynamics invalidates the use of hydrodynamic models. This problem becomes more pronounced as we go to harder x-ray energies. In this paper we propose a hybrid approach that we developed that allows the correct treatment of medium-sized biological samples by combining a continuum model for the bulk of the sample with an all-particle description for the photoelectrons. We will now describe this model and then apply it to particles and membranes, especially focusing on the photoelectron dynamics and energy transfer to the sample, as a function of pulse length, pulse fluence, and x-ray energy.

## DESCRIPTION OF THE HYBRID MODEL

We combined a particle-in-cell (PIC) model to describe the photoelectron dynamics with a continuum atomic kinetics model to describe the evolution of the trapped slow thermal electrons and the ionic charge states. This approach allows us to treat samples of relevant sizes while correctly treating the photoelectron dynamics and their energy transfer to the sample. For the continuum model we assume cylindrical symmetry and that the XFEL beam is unpolarized. Since we are primarily concerned with the photoelectron dynamics, we neglect the expansion of the sample. Our model tracks the temperature and density of the slow electrons and takes all relevant atomic processes

into account [12]. The three-dimensional photoelectron dynamics is described within a PIC model. Every time step, the charges are assigned to a grid, the Poisson equation is solved using a two-dimensional staggered-grid five point scheme in cylindrical coordinates [16], the force on each photoelectron is calculated, and the photoelectrons are propagated. Since the kinetic energy of the photoelectrons is several keV, a classical description is sufficient. For computational efficiency, we limited the number of photoelectrons to $10^6$. If more electrons are generated, we use superparticles with multiple fundamental charges.

The photoelectrons interact with the rest of the sample through electron stopping (inelastic scattering), elastic scattering and Coulomb forces. The photoelectrons are stopped by both the bound and the free electrons. A bound-electron stopping power is calculated every time step using electron impact ionization and excitation cross sections of the ions [17]. A stopping power associated with free electrons is derived from the equilibration time constant of a free electron gas [18]. For colder materials, bound-electron stopping dominates, whereas for highly ionized systems, free-electron stopping is dominant.

To quantify the effect of the photoelectron dynamics on the imaging resolution, we calculated diffraction patterns with and without instant thermalization of the photoelectrons. We populated the sample volume with carbon atoms of the appropriate number density, and let their ionization states evolve in a way that is consistent with the results from the atomic kinetics equations. At the same time, we displace the carbon atoms in random orientations, moving with an average speed that corresponds to the time-dependent ion temperature. Consistent with our damage model, we neglect the macroscopic expansion of the sample. The degree of image degradation is measured by the residual factor $R$ [19] to a resolution of 1.5 Å. In the ideal case, $R = 0$, and $R$ increases as the image quality becomes poorer. For two totally random images, $R \approx 67\%$, and typical $R$ values for x-ray crystallographic data in the protein database are about 20%.

## RESULTS AND DISCUSSIONS

We simulated the evolution of both particles and membranes exposed to high-intensity x-ray radiation. We considered two types of particles, one 30 nm in diameter and height, and another one 50 nm in diameter and height. We also considered three different membrane thicknesses of 10, 30, and 100 nm. The samples are carbonous with a density of 1.3 g/cm$^3$. We assumed currently available XFEL parameters: The x-ray energy was varied between 2 and 8 keV, the pulse length was varied from 1 to 100 fs, the pulse energy was 1 mJ, and the beam diameter was varied between 0.1 and 1.0 $\mu$m. The XFEL pulse was assumed to be constant in time when it is on and to be fully monochromatic. In our analysis we focus on the amount of energy transferred from the photoelectrons to the materials through stopping since the latter is primarily responsible for the sample damage and degradation of the diffraction pattern.

For hydrodynamic models, binary trapping is usually assumed, meaning that photoelectrons either escape the sample when the sum of their kinetic and potential energy is larger than zero, or they are completely trapped, in which case they instantaneously equilibrate. For simple geometries, analytic formulas exist to determine the trapping threshold [20]. Our simulations show that instead of being trapped completely inside the sample, photoelectrons are in general confined only to its vicinity, and, on the timescale of the pulse, can spend a significant amount of time outside of the sample. This alters both the energy transfer and the Coulomb explosion dynamics.

### Particles

We first discuss particles exposed to XFEL pulses. Figure 1 shows scatter plots of the photoelectron positions at different times during the pulse. Photoelectrons are generated throughout the pulse. Whereas the first ones escape, the particle charges up subsequently, and eventually the electrons are confined to the vicinity of the sample. The amount of transferred energy depends super-linearly on the x-ray fluence and particle size since only when the electrons are inside the sample can they transfer energy through stopping. At lower fluences and for smaller particles, the trapped electrons spend only a small fraction of the pulse duration inside the particle, and so transfer only a small amount of energy. At higher fluences and for larger particles, more photoelectrons are being generated, and the photoelectrons are more strongly confined to the sample, so that the energy transfer is more efficient. Therefore, a significantly larger amount of energy is transferred.

We found that the amount of energy transferred from the photoelectrons to the sample can strongly depend on the pulse length. Figure 2 shows the time-integrated transferred energy as a function of the pulse length at 8 keV. For lower fluences, the deposited energy is roughly constant and relatively small since the photoelectrons escape the particle. Energy is transferred only initially when the photoelectrons traverse the sample. When the pulse duration

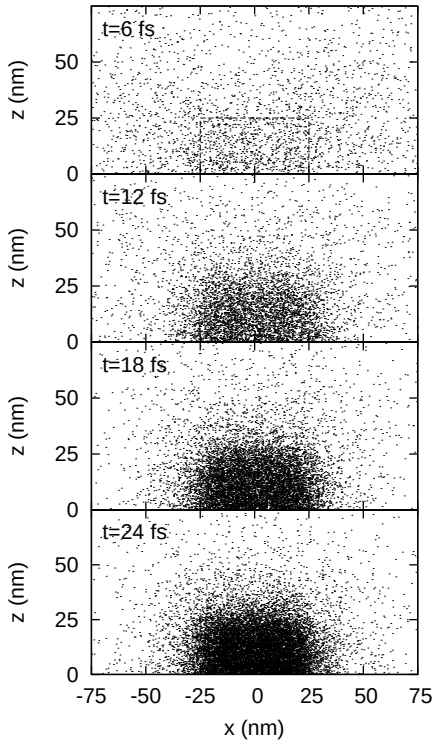


FIG. 1. $x$-$z$ positions of a subset of photoelectrons for a 50 nm particle exposed to an 8 keV XFEL pulse with a duration of 30 fs and 1 mJ pulse energy, focused to 150 nm.

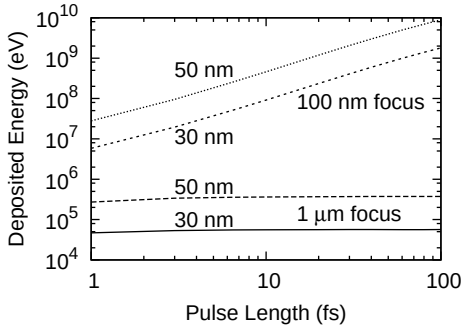


FIG. 2. Total kinetic energy transferred to 30 nm and 50 nm particles for an 8 keV XFEL pulse with a 1 mJ pulse energy and two different focal diameters.

is shorter than the escape time of the photoelectrons, the transferred energy decreases somewhat with pulse length. For larger fluences, the electrons are trapped and reside in the vicinity of the sample, see Figure 1, and transfer energy whenever they traverse the sample. For longer pulses, the photoelectrons traverse the sample more often and so transfer more energy. Note that even 100 fs-long pulses are insufficient for the photoelectrons to equilibrate.

The photoelectron dynamics depends strongly on their initial kinetic energy, which, in turn, depends on the x-ray energy. Figure 3 shows the total transferred energy as a function of the x-ray energy for different beam diameters. For large beam diameters, photoelectron trapping is pronounced only for soft x rays between 2 and 4 keV. Trapping in the case of harder x rays occurs only for smaller beam diameters. Since for soft x rays, the sample opacity sharply decreases when the x-ray beam is more strongly focused, the amount of transferred energy depends sub-linearly on the x-ray fluence. On the other hand, for harder x rays, the opacity does not significantly change during the pulse, and trapping confines the photoelectrons closer to the sample for small focal diameters, leading to a super-linear increase in the amount of transferred energy with fluence.

The transfered kinetic energy, as shown in Figures 2 and 3, corresponds directly to degree of image degradation. The pulse-averaged residual factor $R$ of 30 nm particles exposed to an 8 keV XFEL pulse with a 1 mJ pulse energy

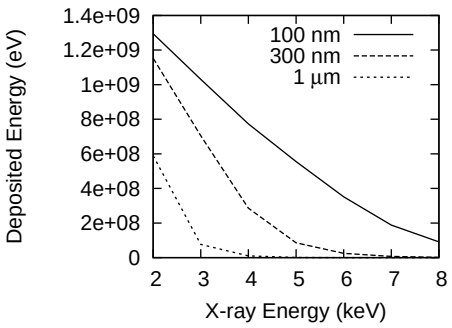


FIG. 3. Total kinetic energy transferred to a 30 nm particle for an XFEL pulse with a duration of 10 fs, 1 mJ pulse energy, and three different pulse diameters.

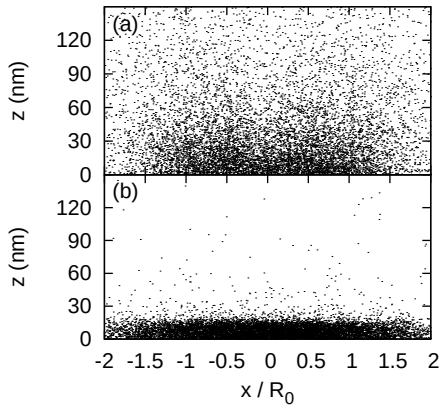


FIG. 4. $x$-$z$ positions of a subset of photoelectrons for a 30 nm-thick membrane exposed to an 8 keV XFEL pulse with a duration of 30 fs and 1 mJ pulse energy, focused to (a) $2R_0$ =1.0 $\mu$m and (b) $2R_0$ =0.1 $\mu$m. $R_0$ is the standard deviation of the Gaussian intensity profile.

and 30 fs pulse length decreases continuously from 10.2% for a 100 nm beam to 1.2% for a 1 $\mu$m beam. The $R$ factor at the end of the pulse ranges, correspondingly, from 46.3% to 4.9%. The pulse-averaged $R$ factor for a 100 fs-long pulse and a 100 nm focus is 14.5%, illustrating the importance of the pulse duration on the image degradation. The pulse-averaged $R$ factor measured in experiments will be larger because our model does not account for macroscopic expansion of the sample due to hydrodynamic and Coulomb forces.

## Membranes

We will now discuss the damage dynamics in membranes. Figure 4 shows scatter plots of the photoelectron positions at the end of 30 fs-long x-ray pulses for two different beam diameters. Unlike in the case of particles, the photoelectrons are trapped even for the bigger 1 $\mu$m focus, albeit the confinement to the membrane is much weaker than for the smaller focus. Similar to the case of particles, a smaller focal spot leads to a larger number of photoelectrons, and to more efficient energy transfer to the membrane due to increased confinement.

The onset of trapping in membranes at relatively low fluences also affects the dependence of the transferred energy on the pulse length, as shown in Figure 5. The high-focus case shows a strong pulse-length dependence since most of the electrons are trapped inside the sample, see Figure 4 (b), and a longer pulse directly translate to more time for the photoelectrons to transfer their energy. For the lower-fluence case, the photoelectrons can also transfer more energy during longer pulses since trapping occurs even for the 10 nm-thick membranes. When the membrane thickness is increased, the photoelectron confinement increases and becomes more similar to the high-focus case.

For the fluences and geometries considered in this study, we found that the electrostatic trapping is sufficiently strong so that the x-ray absorption and the energy transfer profiles roughly trace each other. The energy transfer profile is expected to be larger in extent at very low fluences, which is relevant, for example, for x-ray–beam–imprint

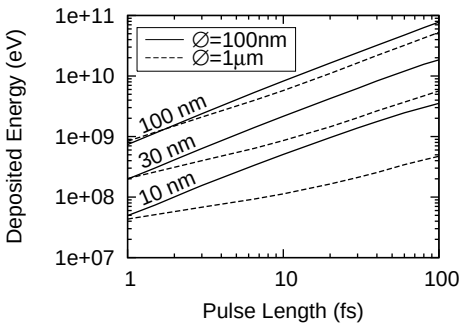


FIG. 5. Total kinetic energy transferred to membranes of three different thicknesses, irradiated by an 8 keV XFEL pulse with 1 mJ pulse energy and two different beam diameters ∅.

studies [21].

## CONCLUSIONS

In summary, we demonstrated that the photoelectron dynamics is pivotal for describing the damage processes since it determines the timescale for the energy transfer from the photoelectrons to the sample that affects ionization, hydrodynamic motion, and local atomic motion. The dynamics also determines the charge distribution that controls the Coulomb explosion. The photoelectrons carry most of the absorbed x-ray energy, but often only a fraction of this energy is transferred to the sample during the pulse. The energy transfer characteristics are strongly pulse-length dependent.

We found that even though positive charging of the sample does lead to electrostatic trapping of photoelectrons, the trapping means a confinement of the photoelectrons only to the vicinity of the sample, thereby altering the energy transfer characteristics and the charge distribution, with the energy transfer depending non-linearly on the x-ray fluence and pulse length. These effects are more pronounced for harder x rays. To describe damage induced by hard XFEL pulses, we need to carefully consider the dynamics of the photoelectrons, for example using the methods proposed in this paper. Hydrodynamic models alone are often insufficient.

## ACKNOWLEDGMENTS

This work was performed under the auspices of the U.S. Department of Energy by Lawrence Livermore National Laboratory under Contract DE-AC52-07NA27344. The author would like to acknowldge useful discussions with Richard London and Matthias Frank.

* hauriege1@llnl.gov

[1] R. Neutze, R. Wouts, D. van der Spoel, E. Weckert, and J. Hajdu, Nature **406**, 752 (2000).
[2] M.M. Seibert *et al.*, Nature **470**, 78 (2011).
[3] H.N. Chapman *et al.*, Nature **470**, 73 (2011).
[4] M. Frank *et al.*, "Improved high-resolution structure determinations of biological macromolecules by combined LCLS CXI and cryo-EM measurements," (2011), LCLS beam time proposal L431.
[5] L. Lomb *et al.*, Phys. Rev. B **84**, 214111 (2011).
[6] A. Barty *et al.*, Nat. Photon. **6**, 35 (2012).
[7] R. Fung, V. Shneerson, D. Saldin, and A. Ourmazd, Nat. Phys. **5**, 64 (2009).
[8] M. Bergh, N. Timneanu, and D. van der Spoel, Phys. Rev. E **70**, 051904 (2004).
[9] Z. Jurek, G. Oszlanyi, and G. Faigel, Europhys. Lett. **65**, 491 (2004).
[10] B. Ziaja, R. A. London, and J. Hajdu, J. Appl. Phys. **99**, 033514 (2006).
[11] B. Ziaja and N. Medvedev, High Energy Dens. Phys. **8**, 18 (2012).
[12] S. P. Hau-Riege, R. A. London, and A. Szoke, Phys. Rev. E **69**, 051906 (2004).
[13] S. P. Hau-Riege, R. A. London, H. N. Chapman, and M. Bergh, Phys. Rev. E **76**, 046403 (2007).

[14] B. Ziaja, A.R.B. de Castro, E. Weckert, and T. Möller, Eur. Phys. J. D **40**, 465 (2006).
[15] C. Caleman, M. Bergh, H. A. Scott, J. C. Spence, H. N. Chapman, and N. Timneanu, J. Mod. Opt. **58**, 1486 (2011).
[16] U. Schumann and R. A. Sweet, J. Comp. Phys. **20**, 171 (1976).
[17] M. Lennon, K. Bell, H. Gilbody, J. Hughes, A. Kingston, M. Murray, and F. Smith, J. Phys. Chem. Ref. Data **17**, 1285 (1988).
[18] J. Huba, *NRL Plasma Formulary* (The Office of Naval Research, 2011).
[19] S. P. Hau-Riege, R. A. London, G. Huldt, and H. N. Chapman, Phys. Rev. E **71**, 061919 (2005).
[20] S. P. Hau-Riege, *High-Intensity X-rays – Interaction with Matter: Processes in Plasmas, Clusters, Molecules, and Solids* (Wiley-VCH, 2011).
[21] J. Chalupský *et al.*, Opt. Express **17**, 208 (2009).